www.sciencemag.org/cgi/content/full/science.1243971/DC1

Supplementary Materials for

The Hippo Signaling Pathway Interactome

Young Kwon, Arunachalam Vinayagam, Xiaoyun Sun,
Noah Dephoure, Steven P. Gygi, Pengyu Hong, Norbert Perrimon*

*To whom correspondence should be addressed. E-mail: perrimon@receptor.med.harvard.edu

Published 10 October 2013 on *Science* Express
DOI: 10.1126/science.1243971

This PDF file includes:

Other Supplementary Material for this manuscript includes the following:
(available at www.sciencemag.org/cgi/content/full/science.1243971/DC1

Tables S1, S2, S6, S7, and S9 as Excel files

Materials and Methods

Generation of stable cell lines for tandem affinity purification

To generate the DNA constructs for tandem affinity purification, we subcloned the coding sequences of *fj*, *d*, *mer*, *hpo*, *sav*, *wts*, *mats*, *ex*, *yki* and *sd* in the pMK33-CTAP vector (*8*). For *ft*, we joined two cDNA fragments, nucleotide 1-411 and 13,705-15,441, with KpnI linker sequence. The resulting fragment (ftΔECD) (*21*), lacking most of the extra cellular domain, was subcloned into pMK33-CTAP. For *ds*, we combined two DNA fragments corresponding to nucleotide 1-270 and 9,079-10,509 of *ds* coding sequence (Q24292, Uniprot) with XhoI linker sequence. The resulting DNA fragment, dsΔECD (*21*), was subcloned into pMK33-CTAP. DNA constructs were validated by sequencing.

S2R+ cells were maintained in Schneider's Insect Medium (Invitrogen) supplemented with 10% heat-inactivated Fetal Bovine Serum at 25°C. To generate stable cells, S2R+ cells were transfected with the pMK33-CTAP constructs using Effectene transfection reagent (Qiagen). Stable cells were selected by exposing the transfected cells to 200 μM Hygromycin (Calbiochem, 40051). Expression of the baits was tested by Western blotting with anti-SBP tag antibody (Santa Crutz, sc-101595) after inducing them overnight with 140 μM $CuSO_4$ (Fisher Scientific).

Tandem affinity purification

Tandem affinity purification was performed as previously described (*7*, *8*) with minor modifications. 1-2 $x10^9$ cells (twelve 150 cm^2 flasks) were induced overnight with 140 μM $CuSO_4$. The cells were collected by centrifugation and washed twice with ice-cold PBS. Cells were lysed by incubating for 15 minutes on ice in 40 ml of lysis buffer consisting of 50 mM Tris-HCl pH 7.5, 5% glycerol, 0.4% NP-40, 1.5 mM $MgCl_2$, 125 mM NaCl, 25 mM NaF, 1 mM Na_3VO_4, 1 mM DTT, 1 mM EDTA and Complete protease inhibitor (Roche, 11697498001). Insoluble fraction from the lysate was removed by precipitating at 27,000 g for 30 minutes.

We incubated the lysates with 500 μl of 50:50 IgG Sepharose 6 (Amersham, 17-0969-01) slurry equilibrated with lysis buffer at 4ºC for 90-120 minutes with rocking. IgG Sepharose was collected by centrifugation at 1,000 rpm for 5 minutes and transferred to Pierce Centrifuge Columns, 5 ml (Pierce, 89897). Subsequently, the beads were washed once with 1 ml of lysis buffer and 4 times with 1 ml TEV cleavage buffer comprising 10 mM Tris-HCl pH 8.0, 150 mM NaCl, 0.05% NP-40, 0.5 mM EDTA and 1 mM DTT. To elute the protein complexes, the column was sealed with caps after addition of 1 ml TEV buffer and 10 μl TEV protease (100 U; Invitrogen, 12575-015) to the beads and rotated overnight at 4 ºC. The TEV buffer (1 ml) inside the column was collected, and the residual protein complexes were eluted twice with 1 ml TEV buffer. The elutes were transferred to a new Pierce Centrifuge Columns, 2 ml (89896), then incubated with 250 μl 50:50 Streptavidin Plus UltraLink Resin (Pierce, 53117) at 4 ºC for 90-120 minutes with rotation. The Resin was washed 5 times with 1 ml wash buffer (10 mM Tris HCl, pH 8.0 and 150 mM NaCl). Purified protein complexes were eluted twice with 250 μl of elution buffer (10 mM Tris HCl, pH 8.0, 1 M NaCl, 2 mM biotin and 0.5% NP-40).

The eluted protein complexes were precipitated with TCA, and then washed once with 10% TCA and three times with Acetone. Trypsin digestion was performed in 30 µl of digestion buffer (100 mM Ammonium Bicarbonate and 10% Acetonitrile) with Sequencing Grade Modified Trypsin (1:40 dilution; Promega, V5113) at 37ºC for 4-5 hours. Digested samples were dried with Speed-Vac and dissolved in Mass Spec buffer (5% Formic Acid and 5% Acetonitrile). Then, the peptides were purified using Zip Tip (Millipore, ZTC18M960) and resuspended in 10 µl of Mass Spec buffer.

LC-MS/MS analysis

All AP/MS experiments for each bait or tag-only control were performed at least in triplicates to increase the quality of data and facilitate statistical analyses.

Typically, 4 µl of peptides resuspended in Mass Spec buffer was analyzed on a LTQ Orbitrap Discovery mass spectrometer (Thermo Fisher Scientific) equipped with an Agilent 1200 binary pump (Agilent Technologies). Peptides were separated on a microcapillary column (125 µm × 18 cm) hand-packed with C18 resin (Magic C18AQ, 5 µm particles, 200 Å pore size, Michrom Bioresources) using a 45 min linear gradient of 5% to 25% (v/v) acetonitrile in 0.1% (v/v) formic acid with an in-column flow rate of 500-800 nl/min. For each cycle, one full high mass resolution MS scan of mass/charge ratio (m/z) = 350 to 1800 was acquired in the Orbitrap with an automatic gain control (AGC) target of 1×10^6 and maximum ion accumulation time of 1 s. Each full scan was followed by the selection of the most intense ions, up to 10, for collision-induced dissociation (CID) and MS2 analysis in the linear ion trap using an AGC target of 2×10^3 and a maximum ion accumulation time of 150 ms. Ions selected for MS2 analysis were excluded from reanalysis for 30 s. Ions with a charge of +1 or with unassigned charge were also excluded from further analysis. Lockmass, with atmospheric polydimethylsiloxane (m/z = 371.1012) as an internal standard, was used in all runs to calibrate orbitrap MS precursor masses.

Database searching and filtering

MS/MS spectra were matched to peptide sequences using SEQUEST (*22*) and a composite database containing the translated sequences of all predicted open reading frames of *D. melanogaster* (ftp://ftp.flybase.net, r5.23) and its reversed complement. Search parameters allowed for up to two missed cleavages, a mass tolerance of 25 ppm, a static modification of 57.02146 Da (carboxyamidomethylation) on cysteine, and a dynamic modification of 15.99491 Da (oxidation) on methionine. Peptide spectral matches were filtered to 1% false discovery rate (FDR) using the target-decoy strategy (*23*) combined with linear discriminant analysis (LDA) (*24*) using several different parameters including the SEQUEST Xcorr and delta-correction (dCn) scores, precursor mass error, and observed ion charge state. Linear discriminant models were calculated for each LC-MS/MS run with peptide matches to forward and reversed protein sequences as positive and negative training data. Peptide spectral matches within each run were sorted in descending order by discriminant score and filtered to a 1% FDR as revealed by the number of decoy sequences remaining in the dataset.

SAINT analysis

To assign confidence scores for protein-protein interactions (PPIs) in the Hippo pull-down data, we applied the Significance Analysis of INTeractome (SAINT) tool (*9*). The SAINT tool (version 2.3.2) was downloaded from http://saint-apms.sourceforge.net/Main.html and implemented locally. The data was pre-processed by removing bait spectral counts values. The program was ran with control IPs option and using default parameters (i.e. niter=1000, lowMode=1, minFold=1, normalize=0). In total, we used 14 control experiments, including 6 TAP-tag controls and 8 baits from a different signaling pathway, the JAK/STAT pathway, as controls. In order to test the performance of SAINT analysis, we created a positive reference set (PRS) and a random reference set (RRS). The PRS includes 21 positive interactions (bait-prey: D-Wts, Ex-Yki, Ft-Dco, Ft-CKIalpha, Hpo-Sav, Hpo-Rassf, Mats-Wts, Sav-Hpo, Sav-Kibra, Sd-Yki, Wts-Mats, Wts-Yki, Yki-Wbp2, Yki-14-3-3epsilon, Yki-14-3-3zeta, Yki-Sd, Yki-Wts, Yki-Ex, Yki-Mop, Yki-Ack, Yki-Tgi) curated from the literature that overlaps with Hippo pull-down data. To construct an empirically relevant RRS, we first compiled a list of 1348 non-specific interactors from raw DPiM dataset (*25*), which is a large-scale AP/MS dataset in *Drosophila*. Non-specific interactors were defined as proteins that pull-down with approximately 1000 experiments in raw DPiM dataset. From this non-specific interactor list, we randomly sampled 1000 RRS sets consisting of interactions between baits and non-specific interactors, existing in the unfiltered Hippo-PPIN (size of each RRS is equal to the size of PRS). We evaluated the SAINT score performance by analyzing both the false and true positive rates at each SAINT score cutoffs. Additionally, we obtained a similar performance when we tested with a RRS set derived from the predicted non-interacting pairs, defined as protein pairs not reported in existing PPI databases (*Drosophila* PPI or interologs) and at least 5 edges distance away in *Drosophila* PPI networks.

RNAi screen

Since the focus of our screen is the functional validation of 153 high-confidence nodes (SS≥0.8) in Hippo-PPIN, we made a few modifications to the screening set up to increase sensitivity and reduce noise. Previous Yki-based reporter assays measured translocation of Yki into the nucleus (*12*) or interaction between Yki and 14-3-3 (*5*) to monitor Hippo pathway activity following overexpression of Yki. As these assays can reduce detection sensitivity, we used an inducible vector, *pMK33*, where the amount of expression can be adjusted by controlling the concentration of $CuSO_4$. For the reporter construct, we subcloned the fusion fragment of the DNA binding domain (*GAL4DBD*; aa.1-147) of yeast *GAL4* and the full-length *yki* coding sequence into *pMK33*. In our focused-RNAi screen, we used 150 μM of $CuSO_4$, which resulted in a moderate expression of GAL4DBD-Yki. Moreover, we controlled the timing of induction to avoid expression of GAL4DBD-Yki before knockdown of target gene, which may increase noise. Thus, we induced GAL4DBD-Yki at 3 days after transfection. In addition, we used *tubulin-Renilla luciferase* instead of *actin5C-Renilla luciferase* for normalization of transfection efficiency and cell viability since actin cytoskeleton and Hippo signaling have been shown to affect each other (*10*). Large-scale screen requires automatic liquid handling as it employs a number of 384-well plates. As imprecise handling a small volume of liquid with an automatic liquid handler can introduce noise to the assay, we

increased the volume of liquid by conducting the screen in 96-well plates and handled liquid manually using multichannel pipettes.

A total of 255 amplicons corresponding to *lacZ* (control) and 150 nodes in the high-confidence PPIN (SS≥0.8) were provided from the *Drosophila* RNAi screening center (DRSC; http://www.flyrnai.org/). We tried to cover each node with two different amplicons if possible. The amplicons were amplified by PCR, and the products were used for dsRNAs synthesis with 5X T7 MEGAscript kit (Ambion) following the protocols available at the DRSC website. 250 ng dsRNA, 20 ng *pMK33-GAL4DBD-yki*, 5 ng *pUAST-firefly luciferase* and 3 ng *tubulin-Renilla luciferase* were co-transfected into $3x10^4$ cells in each well of 96-well plate using Effectene transfection reagent (Qiagen) following the protocol available at the DRSC website. After 3 days of incubation, 150 µM $CuSO_4$ was added to induce *GAL4DBD-yki*. Following 2 days of incubation, values of firefly luciferase and *Renilla* luciferase were measured using Dual-Glo® Luciferase Assay System (Promega). To normalize firefly luciferase value for transfection efficiency and cell number, we calculated relative luciferase units (RLU) by dividing firefly luciferase values by *Renila* luciferase value. A total of six 96-well plates were used to perform the screen in duplicates. The RLU values in a plate were normalized to the average RLU value of *lacZ* RNAi controls (typically 6 wells in a plate). The average fold-change value for each amplicon was calculated by combining the data from two replicates and transformed the data into $\log_2$ fold-change values. To select hits from the RNAi screen, we used the following criteria: 1) genes with individual amplicons that pass the cutoff value of ±0.58 $\log_2$ fold-change (1.5 fold-change) were selected; 2) In case of multiple amplicons passing the cutoff values, we selected the genes with all amplicons scoring in the same direction (removed the genes where different amplicons scores as both positive or negative regulators). Amplicon IDs and their RLU values are available at DRSC website.

Protein complex enrichment analysis

To analyze protein complexes enriched in the Hippo-PPIN, we applied COMPLEAT(*13*), a protein complex-based enrichment analysis tool. COMPLEAT uses comprehensive protein complex resources generated for *Drosophila* by 1) compiling literature based protein complexes and 2) predicting protein complexes from PPI networks. The resource consists of 7713 protein complexes, which cover almost 50% of *Drosophila* proteins. The tool maps the SAINT score values of individual proteins from the Hippo-PPIN to the members of the protein complexes and then calculates a complex score by calculating the interquartile mean:

$$C_{iqm} = \frac{1}{(Q3 - Q1) + 1} \sum_{i=Q1}^{Q3} x_i$$

$$Q1 = \frac{n}{4} + 1 \qquad Q1 \in \mathbb{Z}$$

$$Q3 = \frac{3n}{4} \qquad Q3 \in \mathbb{Z}$$

Where n denotes the number of proteins in the complex and x_i is the SAINT score of the i^{th} protein in the complex. Note that we used the entire network for the COMPLEAT analysis. In case of missing values, i.e. the member of the protein complex is not part of Hippo-PPIN, the protein was assigned a value of 0. Furthermore, a p-value is computed

to estimate the significance of complex scores as compared to 1000 random-complexes of the same size. We performed complex enrichment analysis for every bait individually as well as for the whole network. For each complex, a score is calculated based on the interquartile mean of SAINT scores of individual members (Complex Score). Since the SAINT score indicates the confidence/specificity of a PPI over the entire PPIs recovered through AP/MS, the Complex Score directly corresponds to the confidence of the interaction between a protein complex and Hippo pathway over the entire unfiltered PPIN. The enriched complexes were visualized using the Cytoscape network visualization software (http://www.cytoscape.org/).

Co-immunoprecipitation

1 µg of total DNA was transfected into S2R+ cells in a single well of 6-well plate with Effectene transfection reagent (Qiagen) following manufacturers protocol. After 2 days of incubation, cells were lysed with lysis buffer. 400-600 µg (1-2 µg/µl) of lysate was incubated with Chromotek-GFP-Trap (Allele Biotechnology, ACT-CM-GFA0050), anti-HA agarose (Sigma, A2095) or anti-c-Myc (9E10) agarose (Santa Crutz, sc-40 AC) for 1.5-3 hours at 4 °C to precipitate the protein complexes. The agarose beads were washed 4-5 times with 1 ml lysis buffer. Protein complexes were detected by Western blotting using anti-GFP antibody (Molecular Probes, A6455), anti-Myc-Tag antibody (71D10; Cell signaling, 2278S) or anti-HA antibody (clone 3F10; Roche, 11867423001).

Fly stocks and generation of transgenic flies

en-GAL4, UAS-GFP (II), HMS00006 (*hpo* RNAi) and HMS01137 (*leash* RNAi) were obtained from the Transgenic RNAi Project (TRiP; http://www.flyrnai.org/). *UAS-yki*$^{3S/A}$ (*UAS-yki.S111A.S168A.S250A.V5*, 228817) was obtained from Bloomington *Drosophila* Stock Center.

The full-length coding sequence of *leash* (CG4674) and human Arrdc3 were subcloned into pWALIUM10-roe (TRiP) using gateway reaction. All transgenes were integrated into attP2 site on 3rd chromosome by germ line transformation.

Manipulation of midgut stem cells

We followed the experimental procedures as previously described (*19*). *UAS-GAL80*^{ts}, *esg-GAL4, UAS-GFP* (II) was used to drive expression of transgenes in midgut progenitor cells. Crosses were kept at the restrictive temperature (18°C) to suppress the expression of transgenes. To induce transgene expression, 0-3 days old progenies were placed at permissive temperature (29°C) for 6 or 8 days. During incubation at 29°C, flies were transferred onto fresh food every 2 days. Midguts were dissected in PBS and stained with DAPI in PBST for 30 minutes to visualize nuclei. Maximum projections of 4-6 stacks of images across an epithelial layer were taken with Leica TCS SP2-AOBS confocal microscopy.

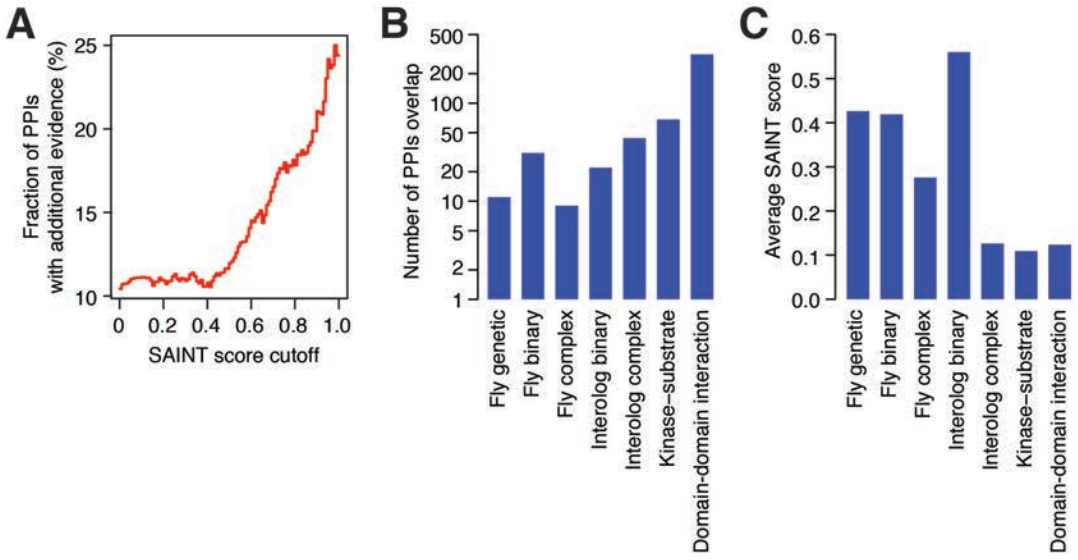

Fig. S1.

Comparison between Hippo-PPIN and a compiled physical and genetic interaction network. We compared the Hippo-PPI network with other physical and genetic interaction networks as previously described (*7*). (**A**) Correlation plot showing the percentage overlap of Hippo-PPIN interactions with published interaction networks at various SAINT score cutoff values. (**B**) The number of Hippo-PPIN interactions overlaps with different interaction networks. Detailed information on the overlaps is in table S3. (**C**) Average SAINT scores for Hippo-PPIN interactions overlapping with different interaction networks. Interestingly, among the overlapping network, the binary interaction retains higher SAINT score, suggesting that Hippo-PPI network is of high quality.

A

Bait	Prey 1	Co-IP	Prey 2	Co-IP
pAGW-Klp61F	*pAWM-wts*	+	*pAWM-fj*	+
pAGW-Thiolase	*pAWM-ftΔECD*	+	*pAWM-dsΔECD*	+
pAWH-hpo	*pAMW-ds-cyto*	+		
pAGW-CG7185	*pAWM-yki*	+		
pAMW-Arf79F	*pAWG-hpo*	+		
pAGW-Sep2	*pAWM-ftΔECD*	+		
pAGW-CG3689	*pAWM-yki*	+		
pAGW-CG5599	*pAWM-wts*	+		
pAGW-HSC70-3	*pAWM-yki*	+		
pAGW-Aats-lys	*pAWM-wts*	+	*pAWM-fj*	–
pAGW-CG8036	*pAWM-mats*	–		
pAGW-CG2186	*pAWM-yki*	+		
pAGW-Dp1	*pAWM-ftΔECD*	–		
pAGW-Hrs	*pAWM-ftΔECD*	+		
pAGW-alpha-adaptin	*pAWM-ftΔECD*	+		
pAGW-Bap	*pAWM-ftΔECD*	+		
pAGW-Sec31	*pAWM-ftΔECD*	+	*pAWM-yki*	+
pAGW-Sec13	*pAWM-ftΔECD*	+		
pAWH-leash	*pAWM-yki*	+		
pAGW-slmb	*pAWM-dsΔECD*	+		
pAGW-CG2943	*pAMW-yki*	+		
pAGW-CG9581	*pAWM-Yki*	+		
pAGW-Atpalpha (not expressed)				
pAGW-Cortactin (not expressed)				

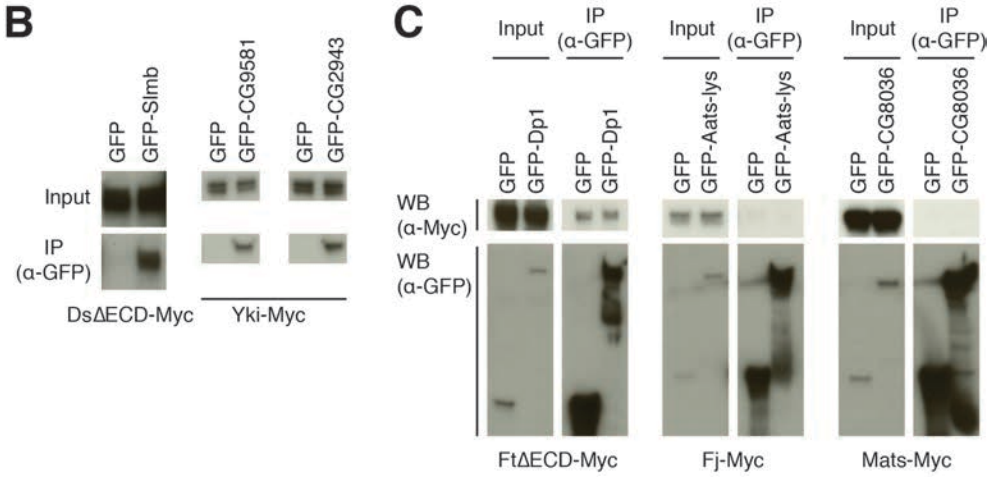

Fig. S2

Experimental validation of 13 % of the high-confidence PPIs with co-immunoprecipitation (co-IP). (**A**) Summary of co-IP experiments. In total, 23 out of 26 tested PPIs were validated. (**B**) Additional co-IP results. (**C**) Co-IP results for three PPIs that failed to validate.

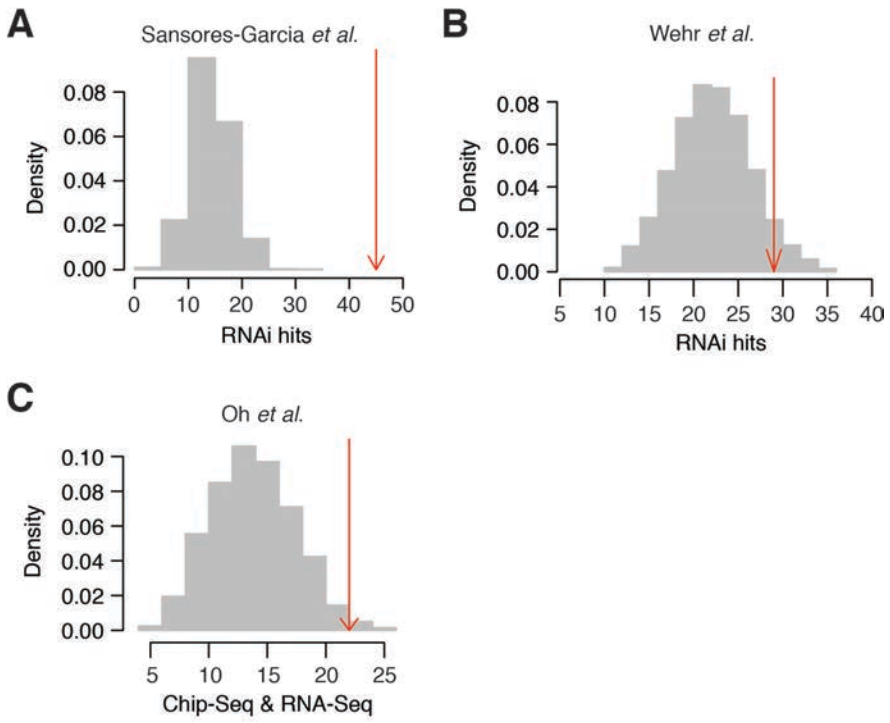

Fig. S3

Comparison with other datasets. (A) Probability density plot. The red arrow indicates the overlap between the high-confidence Hippo-PPIN and the hits from published RNAi screen (Z-score cutoff ±1.5) (*10*) compared to the overlap computed from 1000 random networks of same size and degree distribution (grey bars). The Z-scores were computed for individual plates by using plate mean and standard deviation of the relative luciferase values. (**B**) Probability density plot. The red arrow shows the overlap between high-confidence Hippo-PPIN and the hits from published RNAi screen (Z-score cutoff ±1.5) (*5*) compared to the overlap computed from 1000 random networks of same size and degree distribution (grey bars). (**C**) Probability density plot. Overlap between Hippo-PPIN and potential *yki* regulated genes (yki-Chip-Seq binding data supported by expression changes) (*11*) is shown in red arrow compared to the overlap computed from 1000 random networks (grey bars).

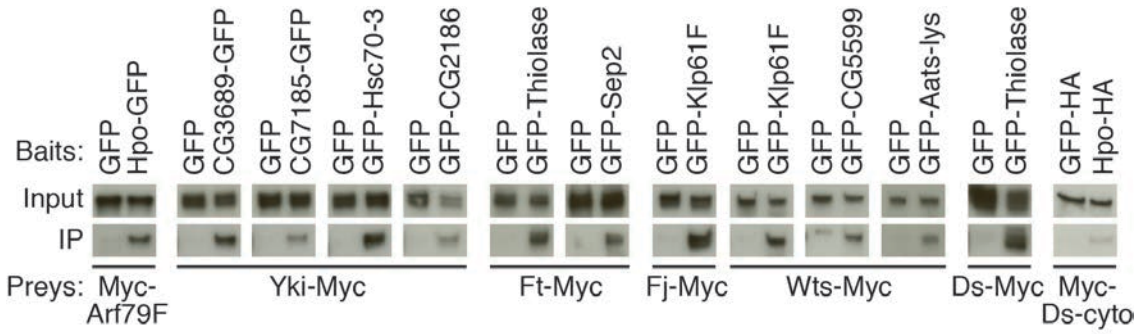

Fig. S4

Co-IP validation of high-confidence PPIs with positive effectors of Yki. We validated 13 PPIs ($\log_2$ fold-change $\leq$-1) with reverse co-IP using the original preys as baits (except Hpo-Ds and Hpo-Arf79F).

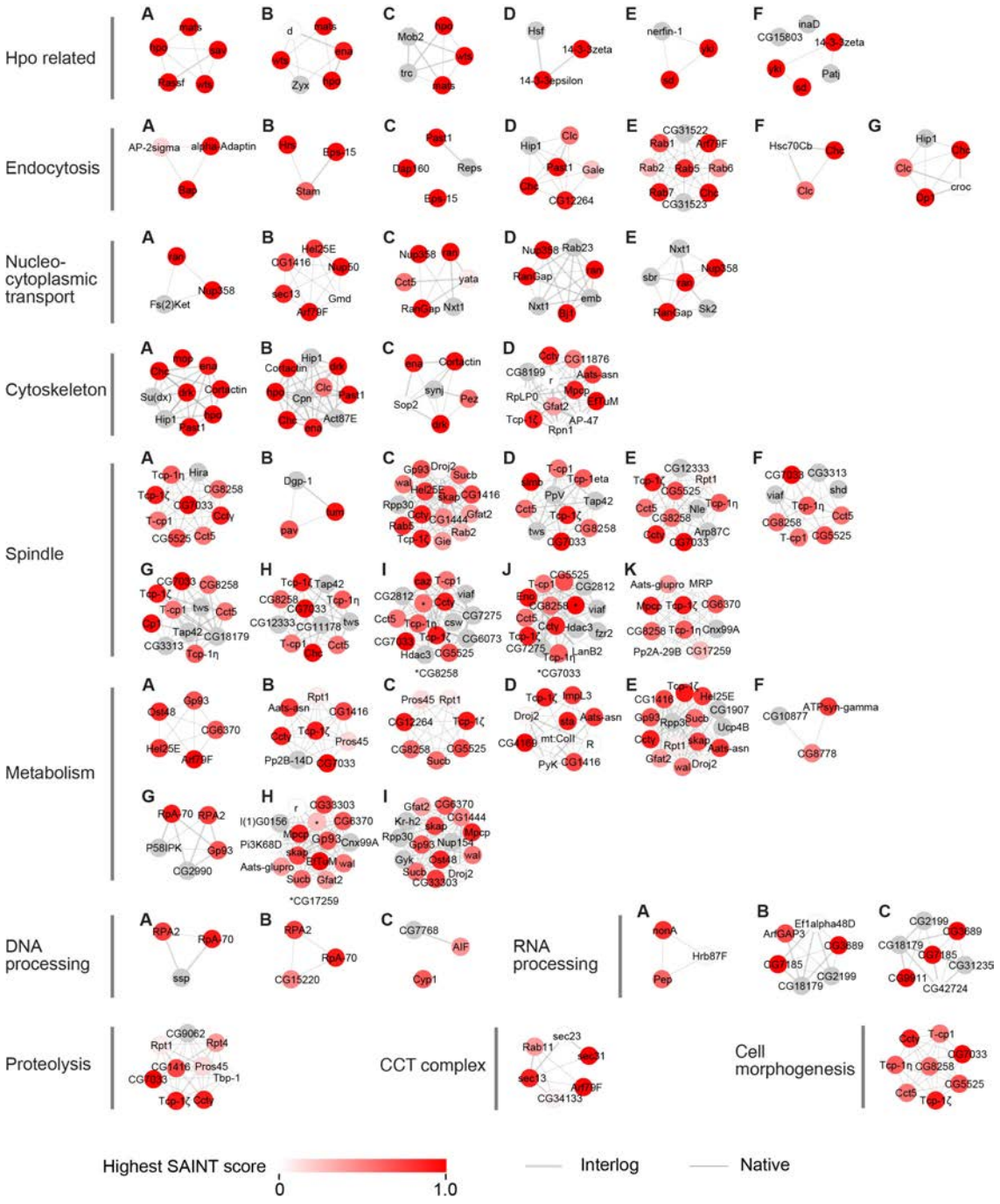

Fig. S5

Sub-complexes identified from Hippo-PPIN. Selected sub-complexes involved in basic cellular processes are shown. Node color represents the highest SS in the entire PPIN. Detailed information can be found in table S7. The full list of sub-complexes is shown in table S6.

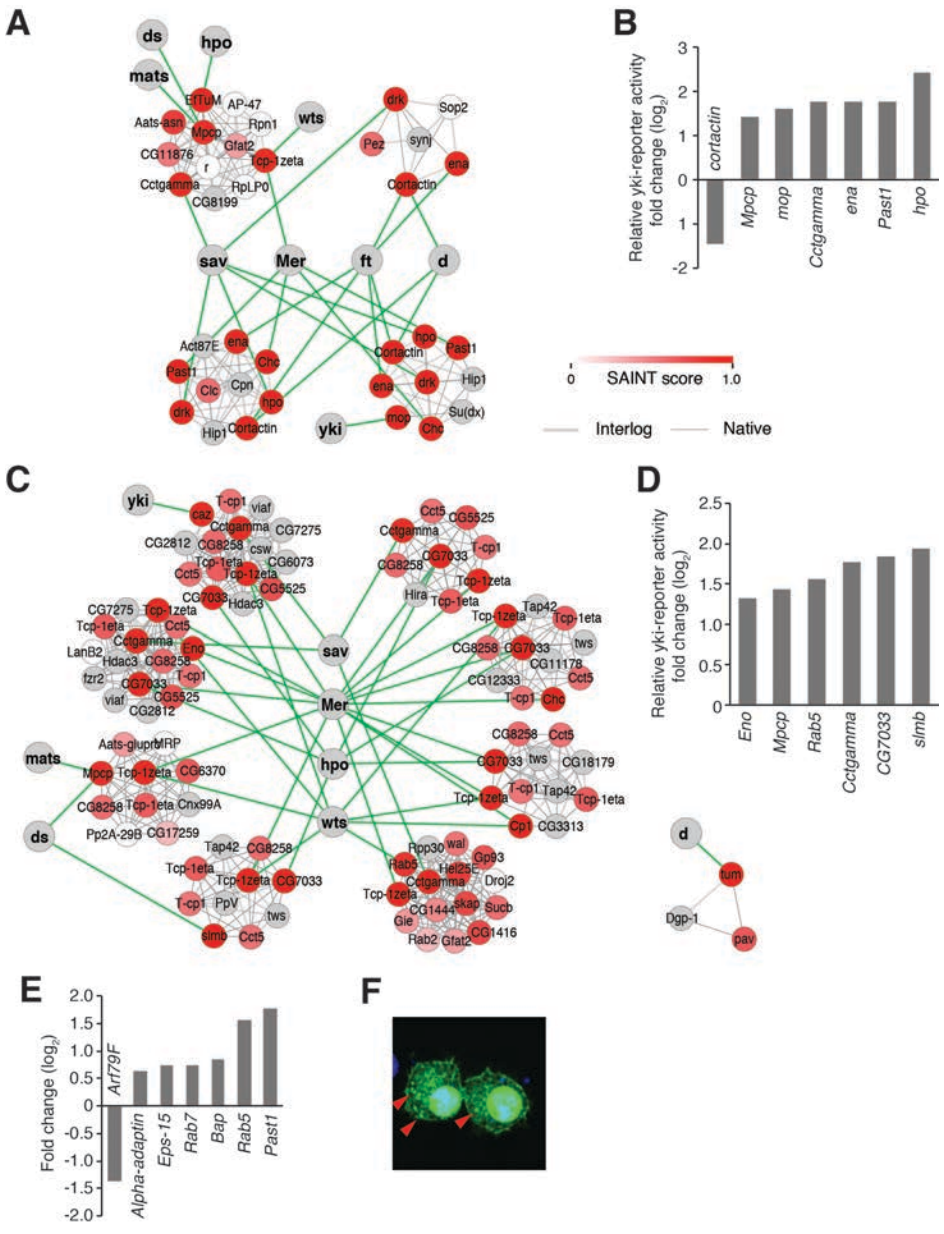

Fig. S6

Interaction networks with sub-complexes involved in organization of actin cytoskeleton (**A**) **and spindle** (**C**)**.** High-confidence interactions with baits (SS≥0.8) are indicated with green edges. Node color represents the highest SS in the entire PPIN. (**B**) Recovery of high-confidence nodes involved in organization of actin cytoskeleton from the RNAi screen. (**D**) Identification of high-confidence nodes in the complexes involved in spindle organization from the RNAi screen. (**E**) Identification of high-confidence nodes involved in vesicle endocytosis and trafficking from the RNAi screen. (**F**) Subcellular distribution of FtΔECD-GFP. We found that FtΔECD (*21*), that is structurally similar to the small cleavage product of Ft, was localized in intracellular vesicles as well as the plasma membrane. Arrowheads indicate intracellular puncta showing FtΔECD-GFP signal. Image was taken 2 days after transfection.

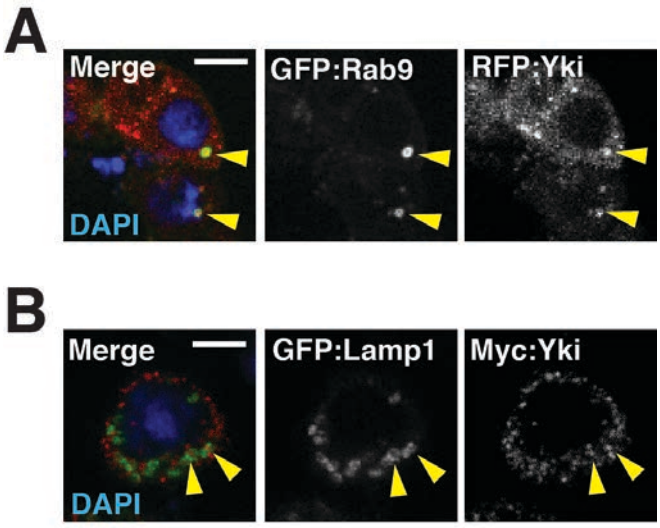

Fig. S7

Co-localization of Yki-containing puncta with Rab9 (A) and Lamp1 (B). Rab9-GFP labels late endosomes, and GFP-Lamp1 shows lysosomes.

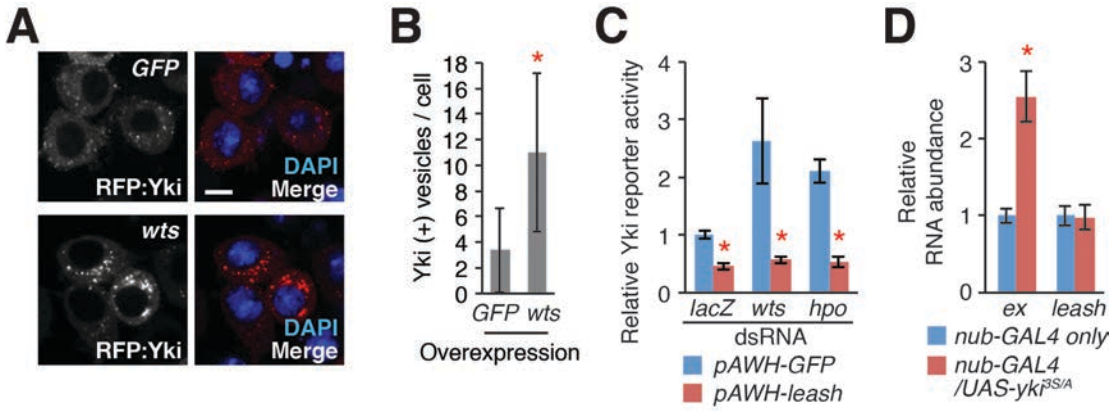

Fig. S8

Regulation of *leash* by Hippo signaling. (**A**) Overexpression of *wts* increased Yki-positive vesicles. (**B**) Quantification of Yki-positive vesicles following *wts* overexpression. (**C**) Knockdown of *wts* did not reverse the reduction of Yki-reporter activity induced by Leash overexpression. All DNAs including Yki-reporter constructs and indicated overexpression constructs were co-transfected along with the indicated dsRNAs. Yki-reporter activity was measured after incubating cells for 3 days. (**D**) Measurement of *leash* mRNA expression upon *yki* activation. Overexpression of an active form of Yki did not change *leash* mRNA expression. An active form of *yki* (*yki*$^{3S/A}$) was induced in the wing discs using *nubbin-GAL4*. *leash* mRNA levels were measured from control (*nubbin-GAL4* only) and *yki*$^{3S/A}$-overexpressed wing discs with quantitative PCR. A transcriptional target of *yki*, *ex* was used as a positive control. All quantification shown are mean±SD. *p≤0.05, Student's t-test.

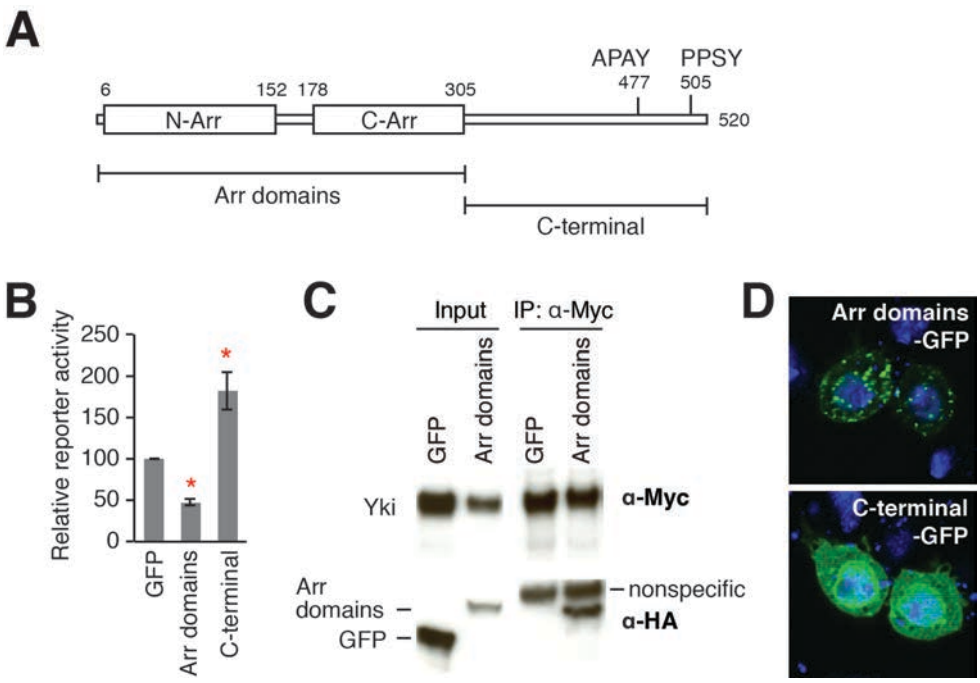

Fig. S9

Leash protein domains study. (**A**) Domain structure of Leash. Conserved N-terminal Arrestin domain (N-Arr), C-terminal Arrestin domain (C-Arr), and putative PPXT motifs (APAY and PPSY) at the C-terminal region are shown. Two deletions, Arr domains (amino acid 1-305) and C-terminal domain (amino acid 306-520), are indicated. (**B**) Yki-reporter assay. Expression of Arr domains reduced Yki-reporter activity. C-terminal domain showed dominant negative effect on Yki-reporter activity. Mean±SDs are shown. Asterisk indicates statistically significant differences between control (GFP) and experiment (Student's *t*-test, $p<0.05$). (**C**) Co-immunoprecipitation. Either GFP-HA or Arr domains-HA is co-transfected with Myc-Yki. Myc-Yki was immunoprecipitated with Sepharose beads conjugated anti-Myc antibody (α-Myc), and co-IP was tested by Western blotting using anti-HA antibody (α-HA). (**D**) Sub-cellular localization of Arr domains. Subcellular distribution of Arr domains-GFP and C-terminal-GFP was tested in S2R+ cells. Arr domains-GFP localized at cytoplasmic punctuated structures/vesicles.

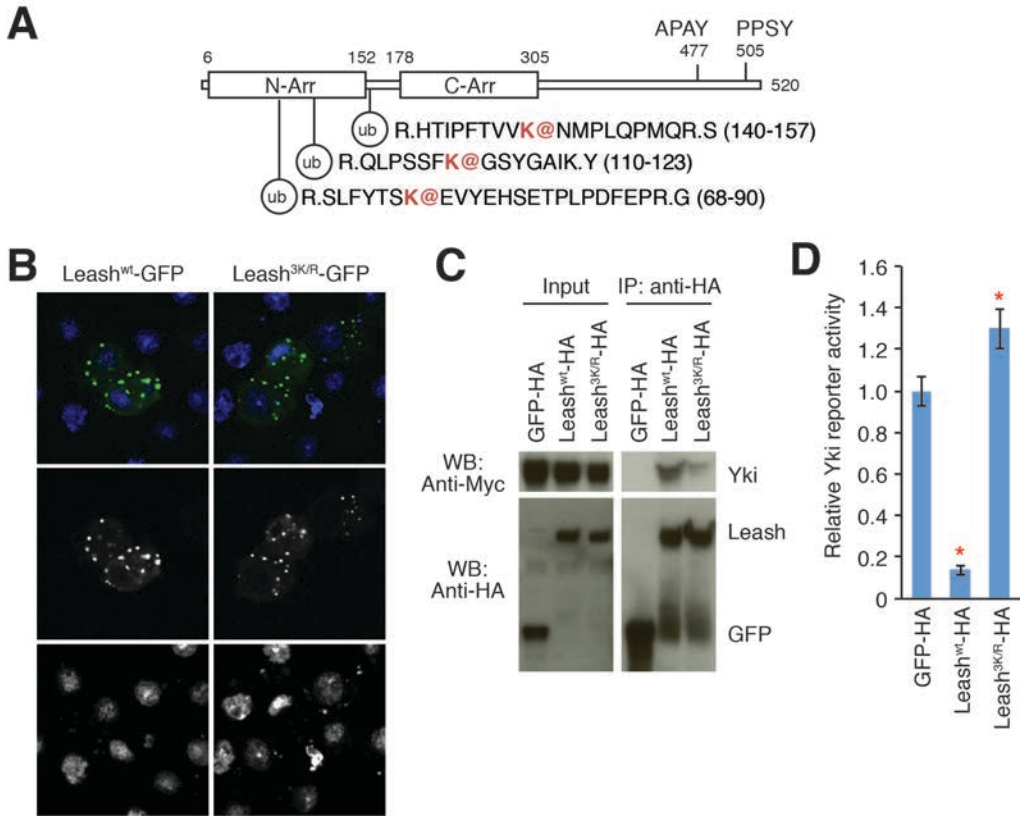

Fig. S10

Regulation of complex formation between Yki and Leash by ubiquitination. (**A**) Three ubiquitinated lysines on Leash identified by mass spectrometry. (**B**) Sub-cellular localization of wild-type and mutant Leash. We generated a mutant version of *leash* (*leash*$^{3K/R}$) by substituting three ubiquitinated lysines to arginines to prevent ubiquitination. The mutations did not affect subcellular localization of Leash. (**C**) Reduction of the interaction between Yki and Leash by amino acids substitution. We performed a co-IP experiment to test the interaction between Yki and Leash$^{3K/R}$. Surprisingly, the mutations greatly reduced the interaction between Yki and Leash. (**D**) Effect of the mutations on the regulation of Yki activity. Overexpression of Leash$^{3K/R}$ did not reduce Yki-reporter activity, which could be explained by the reduced binding between Leash$^{3K/R}$ and Yki. Mean±SDs are shown. Asterisk indicates statistically significant differences between control (GFP-HA) and experiment (Student's *t*-test, $p<0.05$).

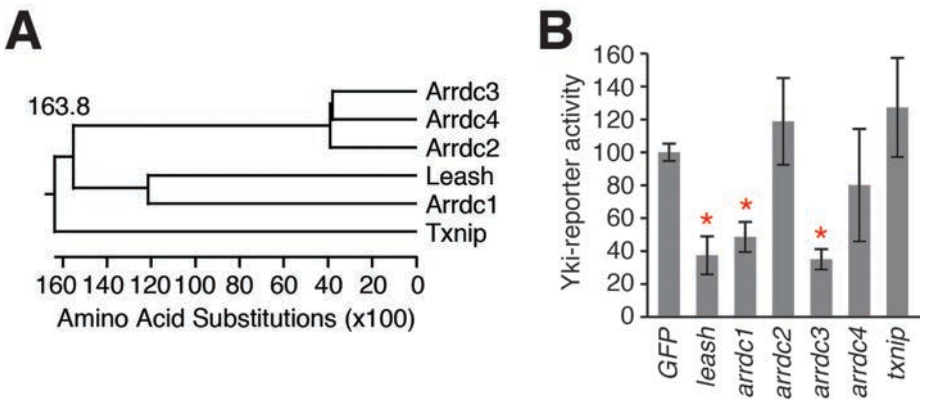

Fig. S11

Regulation of Yki by human Leash orthologs. (**A**) Conservation of Leash in human. The phylogenetic tree is generated with ClustalW. (**B**) Reduction of Yki-reporter activity by the overexpression of human Arrdc1 and Arrdc3. Yki-reporter activity was measured 2 days after transfection. Quantifications shown are mean±SDs. *$p \leq 0.05$, Student's t-test.

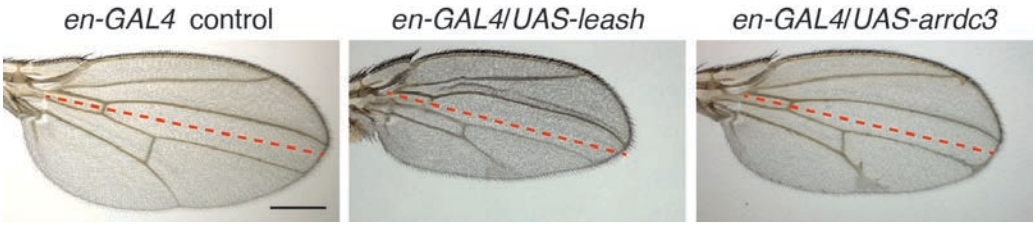

Fig. S12

Leash overexpression reduces wing size. Two copies of *UAS* transgenes were driven by *engrailed-GAL4* at 27°C. Scale bar indicates 300μm.

Table S1. (Separate file)

The entire Hippo-PPIN. Spectral count, number of detection of the peptide(s) mapped to indicated Prey in each AP/MS experiment; SpecSum, sum of Spectral Counts; Spectral Counts in Control, number of detection of the peptide(s) mapped to indicated Prey in each control MS experiment.

Table S2. (Separate file)

Conserved and disease-related nodes (SS≥0.8). Comparison with human disease genes. We searched for human orthologs and disease related orthologs corresponding to 153 high-confidence nodes (SS≥0.8) using DIOPT (http://www.flyrnai.org/cgi-bin/DRSC_orthologs.pl) and DIOPT-DIST (http://www.flyrnai.org/cgi-bin/DRSC_DG_query.pl) tools available at the DRSC website. 98% of the high-confidence nodes are conserved in human. Human orthologs corresponding to ~40% of the high-confidence nodes are implicated in various human diseases.

Table S3.

Overlap between Hippo-PPIN (SS≥0.8) and other physical and genetic interaction networks.

ID1	Symbol1	ID2	Symbol2	SAINT score	Evidence
FBgn0262029	d	FBgn0032731	CG10641	0.96	Domain_Domain_Interaction
FBgn0262029	d	FBgn0002466	sti	0.96	Domain_Domain_Interaction
FBgn0262029	d	FBgn0004167	kst	0.96	Domain_Domain_Interaction
FBgn0262029	d	FBgn0025865	Cortactin	0.97	Domain_Domain_Interaction
FBgn0262029	d	FBgn0250789	alpha-Spec	1	Domain_Domain_Interaction
FBgn0262029	d	FBgn0034264	CG10933	1	Domain_Domain_Interaction
FBgn0262029	d	FBgn0000253	Cam	1	Domain_Domain_Interaction
FBgn0000658	fj	FBgn0028479	Mtpalpha	1	Fly_Complex_PPI
FBgn0001075	ft	FBgn0010909	msn	1	Domain_Domain_Interaction
FBgn0261456	hpo	FBgn0020255	ran	0.99	Domain_Domain_Interaction
FBgn0261456	hpo	FBgn0039055	Rassf	1	Domain_Domain_Interaction
FBgn0261456	hpo	FBgn0023388	Dap160	1	Domain_Domain_Interaction
FBgn0261456	hpo	FBgn0030086	CG7033	0.91	Domain_Domain_Interaction
FBgn0261456	hpo	FBgn0039055	Rassf	1	Fly_Binary_PPI
FBgn0261456	hpo	FBgn0053193	sav	1	Fly_Binary_PPI
FBgn0261456	hpo	FBgn0010411	RpS18	0.8	Fly_Binary_PPI
FBgn0261456	hpo	FBgn0039055	Rassf	1	Fly_Genetic
FBgn0261456	hpo	FBgn0053193	sav	1	Fly_Genetic
FBgn0261456	hpo	FBgn0039055	Rassf	1	Interlog_Binary_PPI
FBgn0261456	hpo	FBgn0035060	Eps-15	0.99	Interlog_Binary_PPI
FBgn0261456	hpo	FBgn0053193	sav	1	Interlog_Binary_PPI
FBgn0261456	hpo	FBgn0020255	ran	0.99	Kinase_Substrate_Prediction
FBgn0261456	hpo	FBgn0039055	Rassf	1	Kinase_Substrate_Prediction
FBgn0261456	hpo	FBgn0035060	Eps-15	0.99	Kinase_Substrate_Prediction
FBgn0261456	hpo	FBgn0000497	ds	0.82	Kinase_Substrate_Prediction
FBgn0038965	mats	FBgn0250814	CG4169	0.99	Interlog_Complex_PPI
FBgn0086384	Mer	FBgn0000317	ck	0.92	Domain_Domain_Interaction
FBgn0053193	sav	FBgn0261456	hpo	1	Fly_Binary_PPI
FBgn0053193	sav	FBgn0030734	CG9911	1	Fly_Binary_PPI
FBgn0053193	sav	FBgn0261456	hpo	1	Fly_Genetic
FBgn0053193	sav	FBgn0261456	hpo	1	Interlog_Binary_PPI
FBgn0003345	sd	FBgn0034970	yki	1	Fly_Binary_PPI
FBgn0003345	sd	FBgn0034970	yki	1	Interlog_Binary_PPI
FBgn0011739	wts	FBgn0004378	Klp61F	0.88	Domain_Domain_Interaction
FBgn0011739	wts	FBgn0011225	jar	0.89	Domain_Domain_Interaction
FBgn0011739	wts	FBgn0014010	Rab5	0.84	Domain_Domain_Interaction
FBgn0011739	wts	FBgn0027329	Tcp-1zeta	0.91	Domain_Domain_Interaction
FBgn0011739	wts	FBgn0261524	lic	0.99	Domain_Domain_Interaction
FBgn0011739	wts	FBgn0010246	Myo61F	1	Domain_Domain_Interaction
FBgn0011739	wts	FBgn0038965	mats	1	Fly_Binary_PPI
FBgn0011739	wts	FBgn0034970	yki	1	Fly_Binary_PPI

FBgn0011739	wts	FBgn0038965	mats	1	Fly_Genetic
FBgn0011739	wts	FBgn0034970	yki	1	Interlog_Binary_PPI
FBgn0011739	wts	FBgn0038965	mats	1	Interlog_Complex_PPI
FBgn0034970	yki	FBgn0003345	sd	1	Fly_Binary_PPI
FBgn0034970	yki	FBgn0011739	wts	1	Fly_Binary_PPI
FBgn0034970	yki	FBgn0004907	14-3-3zeta	1	Fly_Complex_PPI
FBgn0034970	yki	FBgn0036318	Wbp2	1	Interlog_Binary_PPI
FBgn0034970	yki	FBgn0003345	sd	1	Interlog_Binary_PPI
FBgn0034970	yki	FBgn0020238	14-3-3epsilon	1	Interlog_Binary_PPI
FBgn0034970	yki	FBgn0004907	14-3-3zeta	1	Interlog_Binary_PPI
FBgn0034970	yki	FBgn0011739	wts	1	Interlog_Binary_PPI
FBgn0034970	yki	FBgn0035987	CG3689	1	Interlog_Complex_PPI
FBgn0034970	yki	FBgn0003277	RpII215	0.98	Interlog_Complex_PPI

Table S4.

Expected interactions. The expected interactions include experimentally validated PPIs between baits and Hippo pathway components curated from the literature.

Baits	ID1	Hippo pathway components	ID2	Hpo-PPIN	Expression value in S2R+ cells	Expression in S2R+ cells
dachs	FBgn0262029	zyx	FBgn0011642		22.7342	Expressed
ex	FBgn0004583	crb	FBgn0259685		2.28339	Weakly expressed
ft	FBgn0001075	CKIalpha	FBgn0015024	√	202.753	Expressed
ft	FBgn0001075	dco	FBgn0002413	√	71.2113	Expressed
ft	FBgn0001075	lft	FBgn0032230		0.11011	Not expressed
hpo	FBgn0261456	Rassf	FBgn0039055	√	26.0714	Expressed
hpo	FBgn0261456	sav	FBgn0053193	√	12.4462	Expressed
Mer	FBgn0086384	kibra	FBgn0262127		42.1658	Expressed
sav	FBgn0053193	ed	FBgn0000547		0.410783	Not expressed
sav	FBgn0053193	jub	FBgn0030530		18.825	Expressed
sav	FBgn0053193	kibra	FBgn0262127	√	42.1658	Expressed
sav	FBgn0053193	sik2	FBgn0025625		1.06837	Weakly expressed
sav	FBgn0053193	sik3	FBgn0262103		9.82088	Expressed
sd	FBgn0003345	tgi (CG10741)	FBgn0036373	√	149.04	Expressed
wts	FBgn0011739	dachs	FBgn0262029		0.0390587	Not expressed
wts	FBgn0011739	jub	FBgn0030530		18.825	Expressed
wts	FBgn0011739	mats	FBgn0038965	√	49.3926	Expressed
wts	FBgn0011739	sav	FBgn0053193	√	12.4462	Expressed
wts	FBgn0011739	zyx	FBgn0011642		22.7342	Expressed
yki	FBgn0034970	14-3-3epsilon	FBgn0020238	√	3837.02	Expressed
yki	FBgn0034970	14-3-3zeta	FBgn0004907	√	874.138	Expressed
yki	FBgn0034970	ack	FBgn0028484	√	23.518	Expressed
yki	FBgn0034970	ex	FBgn0004583	√	42.6969	Expressed
yki	FBgn0034970	hth	FBgn0001235		0	Not expressed
yki	FBgn0034970	mask	FBgn0043884		28.7124	Expressed
yki	FBgn0034970	mop	FBgn0036448	√	31.0798	Expressed
yki	FBgn0034970	mor	FBgn0002783		120.61	Expressed
yki	FBgn0034970	sd	FBgn0003345	√	28.9369	Expressed
yki	FBgn0034970	Trl	FBgn0003752		144.015	Expressed
yki	FBgn0034970	Wbp2 (CG11009)	FBgn0036318	√	46.1564	Expressed
yki	FBgn0034970	wts	FBgn0011739	√	16.1057	Expressed

Table S5.

RNAi screen results. 103 Hits from the screen are indicated with Fold-change (log2) values. Fold-change (log_2) cutoff is ±0.58 (fold-change ±1.5).

FBgnID	Symbol	Log2 fold change	Z score (RNAi screen; Sansores-Garcia et al.)	Z score (RNAi screen; Wehr et al.)	Log2 fold change for Yki target gene (RNA-seq; Oh et al.)
FBgn0000064	Ald	0.728203993	-	-	1.773552665
FBgn0000253	Cam	0.598363363	-	-	-
FBgn0000317	ck	0.872916501	-	-	-
FBgn0000319	Chc	-	2.346879506	-	-
FBgn0000497	ds	-1.268905512	-	-	1.3344675
FBgn0000578	ena	1.767222171	-	-2.59	-
FBgn0000579	Eno	1.318976153	-	-	-
FBgn0000658	fj	-	-	-	-
FBgn0001075	ft	-	-	-	-
FBgn0001218	Hsc70-3	-0.615871183	-2.556074303	-2.11	-
FBgn0002466	sti	-1.912100668	-	-	1.408906689
FBgn0002638	Bj1	-1.682790769	-	-	-
FBgn0002921	Atpalpha	-1.303551117	-	-	-
FBgn0003022	Ote	-0.763051929	-	-	-
FBgn0003231	ref(2)P	1.180604502	-	-	-
FBgn0003261	Rm62	0.928617007	-1.683312798	2.45	-
FBgn0003277	RpII215	1.321831238	-	2.04	-
FBgn0003279	RpL4	1.098296482	-2.164785625	-	1.630994751
FBgn0003345	sd	1.437275879	2.208984309	-1.88	-
FBgn0003346	RanGap	1.688802828	-	-	-
FBgn0003392	shi	0.585753563	2.311467305	-	-
FBgn0003517	sta	2.814050108	-3.209323768	-	-
FBgn0004167	kst	-	-	-	2.000695589
FBgn0004227	nonA	-	-	-	-
FBgn0004378	Klp61F	-1.007424237	-1.995099345	-	-
FBgn0004583	ex	1.081315078	-	-	2.535940586
FBgn0004638	drk	-	-	2.12	-
FBgn0004907	14-3-3zeta	1.0716351	-	-	-
FBgn0005648	Pabp2	-0.975595879	-2.801474622	-2.57	-
FBgn0010173	RpA-70	1.20192224	-	-	-
FBgn0010246	Myo61F	0.892467825	-	-	2.071000873
FBgn0010348	Arf79F	-1.369508455	-2.360975347	1.55	-
FBgn0010380	Bap	0.836217368	-	-	-
FBgn0010411	RpS18	2.524473887	-3.095837114	-	-
FBgn0010434	cora	1.629417653	-	-	1.595270294
FBgn0010774	Ref1	1.969210328	-	-1.58	-
FBgn0010909	msn	1.439202339	-	-	-
FBgn0011225	jar	-	-	-	-
FBgn0011571	caz	-	-	-	-
FBgn0011704	RnrS	2.052169866	-1.565702936	-1.85	-
FBgn0011739	wts	2.938311132	-	-	-
FBgn0011771	Hem	-2.484292517	-1.177291737	-2.37	-
FBgn0013726	pnut	0.83977325	-	-3.18	1.592448865
FBgn0013770	Cp1	0.917278566	-	-	-

FBgn0014010	Rab5	1.557330023	3.880706166	-	-
FBgn0014029	Sep2	-1.405773533	-	-2.45	-
FBgn0014163	fax	0.789449229	-	-	-
FBgn0014868	Ost48	-	-	-	-
FBgn0015019	Cctgamma	1.763562415	-	-	-
FBgn0015245	Hsp60	1.299254203	-	-	-
FBgn0015795	Rab7	0.745560551	-	-	-
FBgn0016693	Past1	1.771190893	-	-	-
FBgn0020238	14-3-3epsilon	1.02000814	-	-5.72	-1.430717014
FBgn0020255	ran	-	-2.473412763	-	-
FBgn0022343	CG3760	1.680373128	-2.534832951	-	-1.103798007
FBgn0023213	eIF4G	-0.586948437	-1.636307451	-	-
FBgn0023388	Dap160	-	-	-	-
FBgn0023423	slmb	1.938126583	-2.182777456	-	-
FBgn0024238	Fim	-	-	-	-
FBgn0024509	sec13	-	-	2.01	-
FBgn0024556	EfTuM	-	-	-	-
FBgn0024987	ssx	-	-	-	-
FBgn0025352	Thiolase	-1.047835853	-	-	-
FBgn0025457	Bub3	-	-	-	-
FBgn0025637	skpA	0.846088136	-1.90743553	-	-
FBgn0025865	Cortactin	-1.438561922	-	-	-
FBgn0025885	Inos	1.37863803	-	-	-
FBgn0026409	Mpcp	1.426963622	-	-	-
FBgn0027084	Aats-lys	-1.049402066	-1.539742303	-	-
FBgn0027329	Tcp-1zeta	-	-	-	-
FBgn0027598	cindr	0.869619533	-	-	-
FBgn0027616	YT521-B	-	-	-1.69	-
FBgn0027835	Dp1	-	-	-	-
FBgn0028331	l(1)G0289	-	-2.873235512	-	-
FBgn0028479	Mtpalpha	-	-	1.55	-
FBgn0028484	Ack	0.793483405	-	-	-
FBgn0028490	CG31705	1.407017863	-	-	-
FBgn0028734	Fmr1	-	1.605850551	1.64	-
FBgn0029687	Vap-33-1	1.883653337	-	-	-
FBgn0029882	CG3226	1.818269888	2.541507385	-	-
FBgn0029903	pod1	-	3.458155932	-	-
FBgn0030086	CG7033	1.836743778	-1.575040563	-	-
FBgn0030243	CG2186	-2.001775663	1.901409702	2.43	-
FBgn0030612	CG5599	-2.396429534	-	-	1.584282548
FBgn0030734	CG9911	-	-	-	-
FBgn0030808	RhoGAP15B	1.003504867	-	-	-
FBgn0030993	Mec2	-	-	-	-
FBgn0031093	CG9581	3.148415668	-	-	-
FBgn0031450	Hrs	-	-	-	-
FBgn0032393	CG12264	-	-	-1.59	-
FBgn0032731	CG10641	1.596568091	-	-	-1.152633969
FBgn0033062	Ars2	-	-1.993110412	-	-
FBgn0033264	Nup50	-	-	-1.74	-
FBgn0033339	sec31	-	3.119250741	-	-
FBgn0033663	ERp60	-0.598100815	-	-	-
FBgn0033890	Ctf4	-	-	-	1.814911486

FBgn0034264	CG10933	1.770892959	-	-	-
FBgn0034345	CG5174	2.320309653	-	-	-
FBgn0034417	CG15117	2.581598806	2.061696556	-	-
FBgn0034646	Rae1	0.63807191	-	-	-
FBgn0034970	yki	-4.51934164	-	-5.86	-
FBgn0035060	Eps-15	0.736541409	-	-	-
FBgn0035165	CG13887	-	-	-	-
FBgn0035424	CG11505	1.710589316	-	-	-
FBgn0035471	Sc2	0.695454626	-	-	-
FBgn0035600	CG4769	-	-	-	-1.006113754
FBgn0035715	CG10103	1.205097594	-	-	-
FBgn0035811	CG12262	-	-	-1.53	-
FBgn0035872	CG7185	-1.324846847	-	-	-
FBgn0035987	CG3689	-2.119259656	-	-	-
FBgn0036318	Wbp2	-	-	1.67	-
FBgn0036373	CG10741	1.76690474	-	-	-1.353451248
FBgn0036448	mop	1.617195106	-	-	-
FBgn0036451	CG9425	-	-	-	-
FBgn0036892	Lon	0.965656081	-	-	-
FBgn0037312	CG11999	-	-	-	-
FBgn0037530	CG2943	-	-	-	-
FBgn0037607	CG8036	-1.412914974	-	-	-
FBgn0037728	CG16817	0.645828488	-	-1.81	-
FBgn0037756	CG8507	0.597051488	-	-	-
FBgn0037856	CG4674	0.75133972	-	-	-
FBgn0037874	Tctp	0.728463922	2.852546552	-	-
FBgn0037894	Ranbp9	0.901303068	2.063418617	-	-
FBgn0038965	mats	-	5.086414222	-2.22	1.313579273
FBgn0039055	Rassf	-	-	-	-1.548018772
FBgn0039302	Nup358	-0.928343779	-2.32522739	-	1.189425878
FBgn0039713	RpS8	3.458473478	-2.404097173	-	-
FBgn0039776	PH4alphaEFB	1.96391033	-	-	-
FBgn0039924	CG17471	1.965279113	-	-	-
FBgn0041092	tai	1.10487213	-	-	-
FBgn0046214	vig2	-0.619951874	-	-	-
FBgn0051453	pch2	0.600180184	-	-	-
FBgn0052109	CG32109	-	-	-	-
FBgn0053193	sav	1.689570462	3.651542246	-	-
FBgn0063485	Lasp	-	-	-	1.512586672
FBgn0086347	Myo31DF	1.025789711	-	3.23	1.792344056
FBgn0086356	tum	-	-	-	-
FBgn0086384	Mer	-	-	-	-
FBgn0086656	shrb	-	-3.232908443	-	-
FBgn0250789	alpha-Spec	0.682226945	-	-	-
FBgn0250814	CG4169	1.379497195	-1.937880186	-2.12	-1.290304844
FBgn0261014	TER94	0.59825442	-2.104434878	-	-
FBgn0261119	Prp19	-	-1.766583835	-	-
FBgn0261397	didum	1.882609181	-	-	-
FBgn0261456	hpo	2.417009828	3.05165829	-	-
FBgn0261458	capt	-	6.143570934	-	-
FBgn0261524	lic	-	3.047671105	-	-
FBgn0261794	kcc	-	-	-	-

FBgn0262029	d	-	-	-2.62	-
FBgn0263006	Ca-P60A	1.232651314	-1.631413778	-	-
FBgn0263594	lost	-0.681927819	2.093060055	-	-
FBgn0263755	Su(var)3-9	-	-	-	-
FBgn0264855	alpha-Adaptin	0.628935937	4.836568675	-	-

Table S6. (Separate file)

Sub-complexes identified by COMPLEAT analysis. Sub-complexes analyses of (**A**) the entire Hippo-PPIN, (**B**) Ft interactome, (**C**) Ds interactome, (**D**) Fj interactome, (**E**) D interactome, (**F**) Mer interactome, (**G**) Sav interactome, (**H**) Hpo interactome, (**I**) Mats interactome, (**J**) Wts interactome, (**K**) Ex interactome, and (**L**) Yki interactome. Enriched sub-complexes are not present in the Sd interactome. Complex score indicates the interquartile mean of SSs for nodes in a complex. P-value indicates the significance of the complex score compared to the distribution of random complex scores. For each complex 1000 random complexes of same size were generated (used the complex resource as background). Members Gene ID, Members Gene Symbol and Members SAINT Score are listed following the same order.

Table S7. (Separate file)

Sub-complexes involved in basic cellular processes that are shown in fig. S5.

Table S8.

Filtered Leash AP/MS data. HECT ubiquitin ligases, Nedd4, Su(dx) and Lack are highlighted in blue. The Leash-AP/MS identified Yki as an interacting protein. We filtered out proteins identified in 6 CTAP control AP/MS experiments. Top 50 preys are chosen based on the abundance of spectral counts.

Bait_ID	Bait_Symbol	Prey_ID	Prey_symbol	Num of replicates	Spec	Sum of spectral counts
FBgn0037856	CG4674	FBgn0037856	CG4674 (leash)	3	81|66|81	228
FBgn0037856	CG4674	FBgn0259174	Nedd4	3	62|61|52	175
FBgn0037856	CG4674	FBgn0003557	Su(dx)	3	34|30|27	91
FBgn0037856	CG4674	FBgn0039924	CG17471	3	23|24|22	69
FBgn0037856	CG4674	FBgn0029006	lack	3	23|22|20	65
FBgn0037856	CG4674	FBgn0034258	eIF3-S8	3	21|18|24	63
FBgn0037856	CG4674	FBgn0261931	CG42797	3	17|17|11	45
FBgn0037856	CG4674	FBgn0034970	yki	3	17|17|8	42
FBgn0037856	CG4674	FBgn0259785	pzg	3	15|16|11	42
FBgn0037856	CG4674	FBgn0028687	Rpt1	3	12|16|13	41
FBgn0037856	CG4674	FBgn0263006	Ca-P60A	3	14|12|15	41
FBgn0037856	CG4674	FBgn0041180	Tep4	3	14|12|13	39
FBgn0037856	CG4674	FBgn0035688	CG10289	3	14|11|13	38
FBgn0037856	CG4674	FBgn0003676	T-cp1	3	11|12|14	37
FBgn0037856	CG4674	FBgn0264855	alpha-Adaptin	3	13|14|10	37
FBgn0037856	CG4674	FBgn0260962	pic	3	18|10|9	37
FBgn0037856	CG4674	FBgn0023213	eIF4G	3	10|14|10	34
FBgn0037856	CG4674	FBgn0044324	Chro	3	11|13|9	33
FBgn0037856	CG4674	FBgn0002431	hyd	3	13|11|8	32
FBgn0037856	CG4674	FBgn0017545	RpS3A	3	8|11|12	31
FBgn0037856	CG4674	FBgn0010380	Bap	3	12|11|7	30
FBgn0037856	CG4674	FBgn0005632	faf	3	8|12|8	28
FBgn0037856	CG4674	FBgn0261609	eIF-2alpha	3	10|8|9	27
FBgn0037856	CG4674	FBgn0263351	AP-50	3	7|10|8	25
FBgn0037856	CG4674	FBgn0032393	CG12264	3	8|9|7	24
FBgn0037856	CG4674	FBgn0036053	iPLA2-VIA	3	8|10|6	24
FBgn0037856	CG4674	FBgn0032208	CG5604	3	10|6|7	23
FBgn0037856	CG4674	FBgn0037249	eIF3-S10	3	5|7|9	21
FBgn0037856	CG4674	FBgn0035793	CG7546	3	7|8|6	21
FBgn0037856	CG4674	FBgn0037894	Ranbp9	3	7|8|5	20
FBgn0037856	CG4674	FBgn0027571	CG3523	3	8|8|4	20
FBgn0037856	CG4674	FBgn0010078	RpL23	3	6|7|6	19
FBgn0037856	CG4674	FBgn0031310	CG4764	3	7|5|7	19
FBgn0037856	CG4674	FBgn0003279	RpL4	3	5|5|9	19
FBgn0037856	CG4674	FBgn0263594	lost	3	6|7|6	19
FBgn0037856	CG4674	FBgn0262517	l(3)76BDr	3	7|7|5	19

FBgn0037856	CG4674	FBgn0005533	RpS17	3	5|7|6	18
FBgn0037856	CG4674	FBgn0064225	RpL5	3	5|6|7	18
FBgn0037856	CG4674	FBgn0086443	Aats-asn	3	6|6|6	18
FBgn0037856	CG4674	FBgn0029118	Sucb	3	5|8|4	17
FBgn0037856	CG4674	FBgn0053303	CG33303	3	5|7|4	16
FBgn0037856	CG4674	FBgn0003189	r	3	7|5|4	16
FBgn0037856	CG4674	FBgn0025725	alphaCop	3	6|5|4	15
FBgn0037856	CG4674	FBgn0032518	RpL24	3	5|5|4	14
FBgn0037856	CG4674	FBgn0029687	Vap-33-1	3	5|5|4	14
FBgn0037856	CG4674	FBgn0086605	CG9853	3	6|5|3	14
FBgn0037856	CG4674	FBgn0035588	CG10672	3	1|2|11	14
FBgn0037856	CG4674	FBgn0002542	lds	3	3|6|5	14
FBgn0037856	CG4674	FBgn0026562	BM-40-SPARC	3	5|4|4	13
FBgn0037856	CG4674	FBgn0015024	CkIalpha	3	2|6|5	13

Table S9. (Separate file)

COMPLEAT analysis for the Leash interactome. To select for enriched complexes in the Leash interactome, we performed complex enrichment analysis using the entire Leash pull-down data (taking sum of spectral counts from three replicates), and compared it to the complex enrichment of control pull-down. We selected only those complexes that are significant only in the Leash pull-down (p-value cutoff 0.05) compared to control pull-down (p-value cutoff $\geq$ 0.25). Complex score indicates the interquartile mean of spectral counts for nodes in a complex. P-value denotes the significance of complex score compared to 1000 random complexes of same size.

References

1. D. Pan, The hippo signaling pathway in development and cancer. *Dev. Cell* **19**, 491–505 (2010). doi:10.1016/j.devcel.2010.09.011 Medline

2. B. K. Staley, K. D. Irvine, Hippo signaling in *Drosophila*: Recent advances and insights. *Dev. Dyn.* **241**, 3–15 (2012). doi:10.1002/dvdy.22723 Medline

3. G. Halder, R. L. Johnson, Hippo signaling: Growth control and beyond. *Development* **138**, 9–22 (2011). doi:10.1242/dev.045500 Medline

4. E. Cho, Y. Feng, C. Rauskolb, S. Maitra, R. Fehon, K. D. Irvine, Delineation of a Fat tumor suppressor pathway. *Nat. Genet.* **38**, 1142–1150 (2006). doi:10.1038/ng1887 Medline

5. M. C. Wehr, M. V. Holder, I. Gailite, R. E. Saunders, T. M. Maile, E. Ciirdaeva, R. Instrell, M. Jiang, M. Howell, M. J. Rossner, N. Tapon, Salt-inducible kinases regulate growth through the Hippo signalling pathway in *Drosophila*. *Nat. Cell Biol.* **15**, 61–71 (2013). doi:10.1038/ncb2658 Medline

6. F. X. Yu, K. L. Guan, The Hippo pathway: Regulators and regulations. *Genes Dev.* **27**, 355–371 (2013). doi:10.1101/gad.210773.112 Medline

7. A. A. Friedman, G. Tucker, R. Singh, D. Yan, A. Vinayagam, Y. Hu, R. Binari, P. Hong, X. Sun, M. Porto, S. Pacifico, T. Murali, R. L. Finley, Jr., J. M. Asara, B. Berger, N. Perrimon, Proteomic and functional genomic landscape of receptor tyrosine kinase and ras to extracellular signal-regulated kinase signaling. *Sci. Signal.* **4**, rs10 (2011). doi:10.1126/scisignal.2002029 Medline

8. P. Kyriakakis, M. Tipping, L. Abed, A. Veraksa, Tandem affinity purification in *Drosophila*: The advantages of the GS-TAP system. *Fly (Austin)* **2**, 229–235 (2008). Medline

9. H. Choi, B. Larsen, Z. Y. Lin, A. Breitkreutz, D. Mellacheruvu, D. Fermin, Z. S. Qin, M. Tyers, A. C. Gingras, A. I. Nesvizhskii, SAINT: Probabilistic scoring of affinity purification-mass spectrometry data. *Nat. Methods* **8**, 70–73 (2011). doi:10.1038/nmeth.1541 Medline

10. L. Sansores-Garcia, W. Bossuyt, K. Wada, S. Yonemura, C. Tao, H. Sasaki, G. Halder, Modulating F-actin organization induces organ growth by affecting the Hippo pathway. *EMBO J.* **30**, 2325–2335 (2011). doi:10.1038/emboj.2011.157 Medline

11. H. Oh, M. Slattery, L. Ma, A. Crofts, K. P. White, R. S. Mann, K. D. Irvine, Genome-wide association of Yorkie with chromatin and chromatin-remodeling complexes. *Cell Rep* **3**, 309–318 (2013). doi:10.1016/j.celrep.2013.01.008 Medline

12. P. S. Ribeiro, F. Josué, A. Wepf, M. C. Wehr, O. Rinner, G. Kelly, N. Tapon, M. Gstaiger, Combined functional genomic and proteomic approaches identify a PP2A complex as a negative regulator of Hippo signaling. *Mol. Cell* **39**, 521–534 (2010). doi:10.1016/j.molcel.2010.08.002 Medline

13. A. Vinayagam, Y. Hu, M. Kulkarni, C. Roesel, R. Sopko, S. E. Mohr, N. Perrimon, Protein complex-based analysis framework for high-throughput data sets. *Sci. Signal.* **6**, rs5 (2013). doi:10.1126/scisignal.2003629 Medline

14. G. Halder, S. Dupont, S. Piccolo, Transduction of mechanical and cytoskeletal cues by YAP and TAZ. *Nat. Rev. Mol. Cell Biol.* **13**, 591–600 (2012). doi:10.1038/nrm3416 Medline

15. Y. Mao, A. L. Tournier, P. A. Bates, J. E. Gale, N. Tapon, B. J. Thompson, Planar polarization of the atypical myosin Dachs orients cell divisions in *Drosophila*. *Genes Dev.* **25**, 131–136 (2011). doi:10.1101/gad.610511 Medline

16. J. M. Rock, D. Lim, L. Stach, R. W. Ogrodowicz, J. M. Keck, M. H. Jones, C. C. Wong, J. R. Yates, 3rd, M. Winey, S. J. Smerdon, M. B. Yaffe, A. Amon, Activation of the yeast Hippo pathway by phosphorylation-dependent assembly of signaling complexes. *Science* **340**, 871–875 (2013). doi:10.1126/science.1235822 Medline

17. K. M. Draheim, H. B. Chen, Q. Tao, N. Moore, M. Roche, S. Lyle, ARRDC3 suppresses breast cancer progression by negatively regulating integrin beta4. *Oncogene* **29**, 5032–5047 (2010). doi:10.1038/onc.2010.250 Medline

18. G. K. Tofaris, H. T. Kim, R. Hourez, J. W. Jung, K. P. Kim, A. L. Goldberg, Ubiquitin ligase Nedd4 promotes alpha-synuclein degradation by the endosomal-lysosomal pathway. *Proc. Natl. Acad. Sci. U.S.A.* **108**, 17004–17009 (2011). doi:10.1073/pnas.1109356108 Medline

19. P. Karpowicz, J. Perez, N. Perrimon, The Hippo tumor suppressor pathway regulates intestinal stem cell regeneration. *Development* **137**, 4135–4145 (2010). doi:10.1242/dev.060483 Medline

20. F. Ren, B. Wang, T. Yue, E. Y. Yun, Y. T. Ip, J. Jiang, Hippo signaling regulates *Drosophila* intestine stem cell proliferation through multiple pathways. *Proc. Natl. Acad. Sci. U.S.A.* **107**, 21064–21069 (2010). doi:10.1073/pnas.1012759107 Medline

21. H. Matakatsu, S. S. Blair, Separating the adhesive and signaling functions of the Fat and Dachsous protocadherins. *Development* **133**, 2315–2324 (2006). doi:10.1242/dev.02401 Medline

22. J. K. Eng, A. L. McCormack, J. R. Yates, An approach to correlate tandem mass spectral data of peptides with amino acid sequences in a protein database. *J. Am. Soc. Mass Spectrom.* **5**, 976–989 (1994). doi:10.1016/1044-0305(94)80016-2

23. J. E. Elias, S. P. Gygi, Target-decoy search strategy for increased confidence in large-scale protein identifications by mass spectrometry. *Nat. Methods* **4**, 207–214 (2007). doi:10.1038/nmeth1019 Medline

24. E. L. Huttlin, M. P. Jedrychowski, J. E. Elias, T. Goswami, R. Rad, S. A. Beausoleil, J. Villén, W. Haas, M. E. Sowa, S. P. Gygi, A tissue-specific atlas of mouse protein phosphorylation and expression. *Cell* **143**, 1174–1189 (2010). doi:10.1016/j.cell.2010.12.001 Medline

25. K. G. Guruharsha, J. F. Rual, B. Zhai, J. Mintseris, P. Vaidya, N. Vaidya, C. Beekman, C. Wong, D. Y. Rhee, O. Cenaj, E. McKillip, S. Shah, M. Stapleton, K. H. Wan, C. Yu, B. Parsa, J. W. Carlson, X. Chen, B. Kapadia, K. VijayRaghavan, S. P. Gygi, S. E. Celniker, R. A. Obar, S. Artavanis-Tsakonas, A protein complex network of *Drosophila melanogaster*. *Cell* **147**, 690–703 (2011). doi:10.1016/j.cell.2011.08.047 Medline